PROGRESS IN COLOR, COLORANTS AND COATINGS

available online @ www.pccc.icrc.ac.ir

Progress in Color Colorants Coating 19 (2026), 351-361

Ministry of Science, Research and Technology
Institute for Color Science & Technology

Photovoltaic Performance of Photoelectric Dye Sensitized Solar Cell Using Silver Nitrate Doped Titanium Oxide ($AgNO_3$-TiO_2) Nanoparticles as Photoanode Electrode

S. Onyeka Malumi[1], Omamoke O. E. Enaroseha[*2], A. Cynthia Nnanna[3], Obed Oyibo[1], A. Blessing Umukoro[2], R. Daniel-Umeri[1]

[1.] Department of Physics, Southern Delta University, P.O. Box: 2700, Ozoro, Nigeria
[2.] Department of Physics, Delta State University, P.O. Box: 38733, Abraka, Nigeria
[3.] Department of Chemistry, Southern Delta University, P.O. Box: 2700, Ozoro, Nigeria

ARTICLE INFO

Article history:
Received: 05 Oct 2025
Final Revised: 15 Dec 2025
Accepted: 27 Dec 2025
Available online: 16 Feb 2026

Keywords:
Photovoltaic
TiO_2
DSSC
$AgNO_3$

ABSTRACT

In this research, we focused on designing electrode materials that increase the light-harvesting efficiency of photoanodes. Our experimental report presents a new, economical method for producing high-surface-area transition-metal (TM)- doped TiO_2 nanocrystals (NCs) for DSSCs. A Silver nitrate ($AgNO_3$)- doped titanium oxide ($AgNO_3$-TiO_2) was successfully synthesized using the Doctor Blade method and effectively utilized as a photoanode in the fabrication of a dye-sensitized solar cell (DSSC) to study the effect of the dopant on the dye. The solvent method was used to extract the chlorophyll pigment. The absorption study of the sensitized photoanode was characterized using a UV-Vis spectrometer. The DSSC was assembled and tested for photoelectric properties using a solar simulator. The result revealed a photoelectric conversion efficiency PCE (η) of 0.16 %; V_{oc} of 0.452 V, I_{sc} of 0.692 mA/cm^2, V_{max} of 0.324 V, I_{max} of 0.501 mA/cm^2, P_{max} of 0.162 mW/cm^{2,} and FF of 0.52 were obtained. The coated FTO glass with a TiO_2 metal oxide surface, doped with silver at 0.2 molar concentration, has been shown to provide more surface area for dye adsorption and to extend visible light absorption. Prog Color Colorants Coat. 19 (2026), 351-361© Institute for Color Science and Technology.

1. Introduction

Scientists' efforts to stabilize and improve the efficiency of dye-sensitized solar cells (DSSCs) have prompted the solar research community to adopt novel strategies [1-3]. Finding new energy sources with the least toxicity has been one of the biggest problems over the past 10 years [4]. The energy from the sun is the best source of clean, eco-friendly, renewable energy on Earth [5]. DSSCs are simple devices that convert solar energy into electrical energy, based on the groundbreaking discovery of Gratzel [6]. Compared to silicon solar cells, DSSCs are a more affordable and environmentally friendly photo-voltaic technology [7]. Recently, several studies have been conducted to improve power conversion efficiency [8, 9].

The Photosynthesis cycle [10-12], which occurs when plant pigments absorb light photons within the thylakoid membrane, allows living plants to generate bioelectricity by converting sunlight into electricity. In addition to facilitating electron transport, chlorophyll pigments absorb light mostly in the visible range of solar radiation. The photosynthetic cycle depends on carotenoids, which also help the chlorophyll molecule absorb light and enhance its ability to do so [13]. An

*Corresponding author: * enarosehaomamoke@gmail.com
https://doi.org/10.30509/pccc.2025.167687.1457

electron can travel swiftly across a cell's membrane due to solar energy. In solar cells, the absorbed photon is also likely lost when the electron returns to its starting place. Studies have been conducted on these artificial solar cells, which are photovoltaic power generators with high photon capture and charge-separation efficiencies. The DSSC is one of several solar cells under development. Dye-sensitized solar cells (DSSCs) are photovoltaic devices that use the principle of photo-sensitization of a wide band gap semiconductor to convert solar light into electrical power [14]. DSSCs based on natural dyes are recognized in research for their easy fabrication, low production costs, use of flexible conducting substrates, and environmentally friendly nature, despite their known low conversion efficiencies and limitations related to liquid electrolytes [15-18].

In general, photovoltaics absorb photon energy from the sun above a threshold energy, known as the "energy gap" or bandgap; photons with higher energies are absorbed, while those with lower energies pass through the absorber. When the photon energy exceeds the threshold, absorption occurs in organic molecules. The molecular system enters an excited state upon this absorption, producing electrons and holes. In the process of creating dye-sensitized solar cells, naturally derived pigments from leaves, flowers, and fruits exhibit a variety of colors.

Due to their stability, affordability, and photovoltaic properties, TiO_2 nanoparticles are widely used as photoanodes [19]. However, the performance of DSSCs may be negatively impacted by the electrons in TiO_2 nanoparticles recombining with the dye. Numerous studies have altered the surface and photoelectronic properties of photoelectrodes to increase their efficiency [20-25]. Doping TiO_2 with other substances is one way to achieve this. By boosting their absorbance and shifting them into the visible region of the solar spectrum, these techniques expand the range of solar light the photoanodes can absorb. In the end, this can increase the power conversion efficiency by preventing electron-hole recombination [26, 27]. The commercialization of metal-doped TiO_2 nanoparticles in DSSCs is highly promising. To improve the overall effectiveness of DSSCs, these nanoparticles have been synthesized in various ways and with varying dopant concentrations. Compared with pure TiO_2 nanoparticles, the produced nanoparticles exhibit improved physical properties. For example, it has been shown that tungsten-doped nanostructured anatase TiO_2 has 100 times more photoactivity under visible light than nondoped TiO_2 nanoparticles. This is because tungsten can form an energy level within the TiO_2 band gap, thereby serving as a reactive site for the absorption of visible light [28].

The present study reports the photoanode performance and structural characterization of a DSSC doped with silver nitrate at 0.2 M and sensitized with a plant dye extract from *Celosia argentea*. *Celosia argentea,* commonly known as, Shokotor yokotor in the Isoko language, Lagos spinach, *Shoko* in the Yoruba Language, or Nigerian spinach, is a leafy vegetable mainly popular in the western part of Nigeria. It belongs to the family of Amaranthacea. The plants are usually erect, coarse, simple, and branched, with a height of about 0.5 to 1.5 m [29].

2. Theoretical framework

2.1. Optical characterization of film

The films were characterized for their optical properties using a UV-Vis-NIR spectrophotometer, with wave-lengths ranging from 200 to 1100 nm.This was done to determine the absorbance, reflectance, transmittance, refractive index, absorption coefficient, optical thickness, energy band gap, and optical conductivity of the natural dyes used for the sensitization of the substrate. This can also be done by substituting either the absorbance reflectance, or transmittance values into the various equations listed below (Eq. 1);

$$A + T + R = 1 \quad (1)$$

Where A is the absorbance, R is the reflectance, and T is the transmittance, given by equation 2 shows the relationship between the transmittance (T) and absorption (A) of the dye [30],

$$\text{Absorption, } A = 2 - log(\%T) \quad (2)$$

where % T shows the transmittance percentage of light (Eqs. 3-5).

$$\text{Transmittance, } T = 10^{A} \quad (3)$$

$$\text{Reflectance, } R = 1 - (A + T) \quad (4)$$

$$\text{The refractive index (n)} = \frac{1}{Ts} + \sqrt{\frac{1}{Ts^{-1}}} \quad (5)$$

where T_s is the percentage transmittance (Eq. 6).

$$\text{Optical thickness (t)} = \frac{ln\left(\frac{1-R^2}{T}\right)}{\alpha} \quad (6)$$

where T is the transmittance, R is the reflectance, and α is the coefficient of absorption.

Experimentally, the absorption coefficient (α) can be calculated from the simple relation (Eq. 7) [31]:

$$Absorptioncoefficient, \alpha = \frac{1}{d} ln\left(\frac{1}{T}\right) \quad (7)$$

where t represents the thickness of the thin film, T and R are the transmittance and reflectance, respectively. From equation 4, the band gap energy (E_g) of the transparent films is determined by using (Eq. 8) [32]:

$$\alpha h\upsilon = A\left(h\upsilon - E_g\right)^n \quad (8)$$

where A is a proportionality constant, dependent on the properties of material use, the absorption coefficient is represented as α, hυ represents the photon energy, and n represents a constant value, equal to ½ for a direct band gap semiconductor. The energy band gap of the materials will be obtained by extrapolating the linear part of the curve $(ahv)^2 = 0$ in a graph of $(ahv)^2$ against hv (Eq. 9).

$$\text{Optical conductivity,} (\sigma) = \frac{\propto nc}{4\pi} \quad (9)$$

Where α represents the coefficient of absorption, n shows the refractive index, and c is the light speed.

2.2. Morphological characterization of DSSC

The surface morphological characterization of the sensitized TiO_2 photoanode was investigated using a Scanning Electron Microscope (SEM) (JSM-7100F, JEOL.COM) at a magnification of 20.0 kx and a view field of 10.4 µm. The elemental analysis of the TiO_2 photoanode was studied using energy-dispersive X-ray spectroscopy (EDX).

2.3. Structural characterization of DSSC

The structural characterization of the dyes was obtained to study their crystal structures and interplanar spacings using X-ray diffraction (XRD) for cell sensitization. The generated data were used to evaluate several structural factors, including crystallite size, dislocation density, d-spacing, and lattice parameters (a and c). XRD patterns were used to determine the crystallite size of the thin films using Debye Scherrer's formula in equation 10 [33].

$$D = \frac{K\lambda}{\beta cos\theta} \quad (10)$$

where D shows the crystallite size, λ is the wavelength of the X-ray used, k represents a constant given as 0.94, the full width half maximum (FWHM) is represented as β of the XRD peak and θ is the angle of diffraction.

Equation 11 was used to determine the dislocation density δ, which provides additional information on the quantity of faults in the films.

$$\delta = \frac{1}{D^2} \quad (11)$$

The lattice parameters (a and c) of the films were calculated using equations 12 and 13, respectively.

$$a = \frac{\lambda}{\sqrt{3}sin\theta} \quad (12)$$

$$c = \frac{\lambda}{sin\theta} \quad (13)$$

The inter-planar spacing was calculated using the relation (Eq. 14) [34],

$$d_{hkl} = \frac{n\lambda}{2sin\theta} \quad (14)$$

where λ is the X-ray wavelength, n is the order of diffraction, which is typically 1, and θ is the Bragg diffraction angle at peak location, expressed in degrees.

2.4. Electrical characterization of sensitized film

The electrical characteristics of the DSSC were evaluated using a xenon (Xe) lamp solar simulator under white-light illumination at 100 mW/cm^2. The digital source meter measures the short-circuit current (I_{sc}) and open-circuit voltage (V_{oc}). The results were plotted in an I-V curve. The current-voltage (I-V) characterization of the DSSC was studied. From the I-V curve, the maximum power (Pmax), maximum current (Imax), maximum voltage (Vmax), fill factor (FF), and PCE were obtained.

2.4.1. Open-circuit voltage (V_{oc})

When no current is flowing through the cell, the measured cell voltage is known as the V_{oc}. It is the highest voltage (V_{max}) that a solar cell can produce

when there is no resistance between the working and counter electrodes. This illustrates the difference between the semiconducting oxide's Fermi level and redox potential.

2.4.2. Short-circuit current (I_{sc})

Because there is no voltage difference between the electrodes, the cell's output current, or Isc, is zero. Stated otherwise, it is the current that the cell produces when the load resistance is zero. The short-circuit density (Isc), the ratio of the measured short-circuit current, is typically used to express it.

2.4.3. Fill factor (FF)

The FF is the proportion of the maximum output power(Pm) to the result of I_{sc} and V_{oc}. The fill factor, ff, can then take values between 0 and 1. This shows the extent of the electrochemical and electrical losses during DSSC operation (Eq. 15) [35]. Hence,

$$FF = \frac{Pm}{(IscxVoc)} = \frac{I_m \times V_m}{(I_{sc} \times V_{oc})} \quad (15)$$

where I_{sc} is the photocurrent, V_{oc} is the photo-voltage, and Pm is the maximum power point.

2.4.4. Photo- conversion efficiency (PCE)

The photoconversion efficiency (Ƞ) calculates the power output, intensity, and photoconversion efficiency of incident (radiant) light into electrical energy (Eq. 16). [36].

$$n = \frac{I_{sc} \times V_{oc} \times FF}{p} \times \frac{100}{1} \quad (16)$$

where P is the power input.

3. Experimental

3.1. Materials

Materials used in this research are 100 and 200 mL glass beakers, glass rod, masking tape, ceramic mortar and pestle, model: HK-DC-320AS weighing scale, aluminum foil, syringes, filter papers, distilled water, liquid iodide redox electrolyte, crocodile clips, Rheostat, negative and positive terminal probes (wire), glass slides, diamond cutter, magnetic stirrer, Electric Heated Blast dry Box (Oven SM-9023), Ultrasonic machine, thermostatic blast oven with temperature range of 50 °C, ohmnmeter, Fluorine doped tin oxide (FTO) glass, 3g of Titanium Oxide (TiO_2) powder, Silver nitrate ($AgNO_3$), acetone, 2.5 L of methanol and the *Celosia argentea* dye extract. The compounds used in this research were of analytical grade unless stated otherwise. These were used in addition to the usual characterization equipment: UV-Vis-NIR spectro-photometer, 350 W Xenon lamp Solar Simulator, Scanning Electron Microscopy (JSM-7100F, JEOL .COM), X-ray diffractometer (XRD).

3.2. Extraction of dye from dry *Celosia argentea*

The fresh leaves of *Celosia argentea*, as shown in Figure 1, were harvested from a local Agricultural farm in Abraka, Delta State, Nigeria. These leaves were rinsed thoroughly with distilled water to remove dirt particles from the plant surface and air-dried until they became invariant in weight for 2 weeks at a room temperature range of 24 32 °C. The leaves were ground in an electric blender to form a powder. 50 g of each ground leaf was measured using a weighing scale and placed in a 500 mL beaker. They were soaked in 100 ml of methanol and stirred on a magnetic stirrer for 3 hours, then covered with an aluminum foil sheet and set aside for 24 hours. The dyes from the leaves are then extracted into a beaker using Whitman filter paper. The filtered samples are poured into storage containers and kept out of direct sunlight. This is to prevent dye degradation. After filtering, the samples are placed in storage containers and shielded from light. This is to stop the colors from deteriorating [37]. The solvent extraction technique was employed for the isolation of the pigment from Celosia argentea because it efficiently isolates light-absorbing natural pigments, preserves the photo-chemical properties of the dye, is very sensitive to TiO_2, is simple, low-cost, and eco-friendly.

Figure 1: Fresh Celosia argentea leaves.

3.3. Preparation of substrate (FTO glass)

Before cell development, the FTO glass was cleaned by immersing it in an ultrasonic bath for 30 minutes each in distilled water and acetone. This was done to dissolve any unwanted organic materials and remove any dust or contaminants that might have gotten onto the substrate during manufacturing. To aid in removing the acetone initially applied to the substrate, as well as the materials the acetone was unable to clear, methanol is added after another 20 minutes of ultrasonic bathing. To prepare the substrate for deposition, it was heated to 50 °C in a hot-air oven.

3.4. Synthesis of $AgNO_3$-TiO_2 nanoparticle

Using the Doctor Blade technique, a TiO_2 thin-film electrode (photoanode) was developed. To mechanically separate aggregated TiO_2 particles, 3 g of TiO_2 powder was ground and stirred with a pestle while 5 mL of methanol was added dropwise in a mortar to form the TiO_2 paste. During the cell fabrication process, 0.2 mol silver nitrate ($AgNO_3$) was used to dope the TiO_2. The silver nitrate ($AgNO_3$) was dissolved in 2 mL of methanol before adding to the TiO_2 paste.

The substrate for the deposition was a transparent fluorine-doped tin oxide (FTO) conducting glass measuring an average of 2.25 cm by 2.35 cm. The TiO_2/silver nitrate ($AgNO_3$) and TiO_2/Nickel (II) Chloride ($NiCl_2$) paste was applied to the FTO substrate. An ohmmeter was used to check for conductivity on the glass. Two transparent FTO-conducting glasses were used during deposition. While one serves as the depositing surface, the other serves as a guide to ensure uniformity. Paper tape was applied on the conductive side to mask 0.15-0.2 cm at the three edges of the depositing glass surface and the opposite sides of the guiding slide. A glass rod is used to ensure that there is no opening into the masked edges. The substrate was evenly covered with drops of the TiO_2 colloidal solution, which were then evenly spread out using a glass stirring stick. The grown films were annealed at 250 °C for 30 minutes in a thermostatic blast resettable oven with a temperature range of 50 to 1000 °C. After which it was kept to cool and ready for sensitization [38, 39].

3.5. Dye deposition

Glass films coated with TiO_2/Silver Nitrate ($AgNO_3$) were immersed separately in the produced dye extracts for approximately 24 hours throughout the dye deposition process. The sample is put on a rack with the stained surface facing up after the stained TiO_2/silver nitrate ($AgNO_3$) coating is removed with a thong.

3.6. Assembling of DSSC

Assembling a DSC involves sandwiching the photo-anode with the counter electrode. The counter electrode was made from another conductive glass. The glass's conductive side was checked using an ohmmeter. The conductive side of the glass substrate is coated with a carbon pencil, which provides a carbon layer that can serve as the catalytic surface for the redox couple [41, 42]. Since this electrode didn't require tape or masking, its entire surface was covered to maximize its surface area. The KI/Iodine electrolyte solution from the Institute of Chemical Education (ICE) was used as redox electrolyte. On a laboratory table, each dye-stained TiO_2/silver nitrate ($AgNO_3$) electrode was positioned with the film side facing up. The counter electrode was then positioned on top of the electrode, with its conductive side in direct contact with the TiO_2/silver nitrate ($AgNO_3$) film. The two opposing glass slides were positioned so that the counter electrode covered the entire surface of the TiO_2/silver nitrate ($AgNO_3$) and left the 0.2 cm strip of glass uncoated. The slides were held together at the opposite edges with two crocodile clips. An electrolyte solution of potassium iodide-iodine (KI/ Iodine) was introduced through the edges of the slides. The finished solar cell was measured to examine its current and voltage properties.

4. Results and Discussion

4.1. Optical characterization

The absorbance study of TiO_2 /$Ag_{0.2}$/dyes extracted from *Celosia argentea* is shown in Figure 2. The figure shows that the dye's optical absorption decreases with increasing wavelength. The dye-sensitized material exhibits a noticeable peak/increase in the broad absorption spectrum between 620 and 720 nm in the visible light region, indicating the absorption of red light. Across the infrared region, photon absorption was also observed in Figure 2, showing their suitability for the fabrication of infrared devices and devices that will function effectively with red light. *Celosia argentea*

chlorophyll extract is a good photosensitizer for DSSC applications.

Figure 3 shows the transmittance spectra of TiO_2/$Ag_{0.2}$/dye material. With increasing wavelength, transmittance increases. The dye-sensitized material displays a broad peak at 610 nm, ranging from 620 to 740 nm in the visible region, which then broadens and shifts to the infrared region of the electromagnetic spectrum with ageing. The clearly visible surge indicates that the cell has transmitted all wavelengths from 300 to 1100 nm, except red light, which shows the least transmittance in the 640-700 nm range. The surge in transmittance observed in the visible light region suggests that Celosia argentea is suitable for photovoltaic device applications.

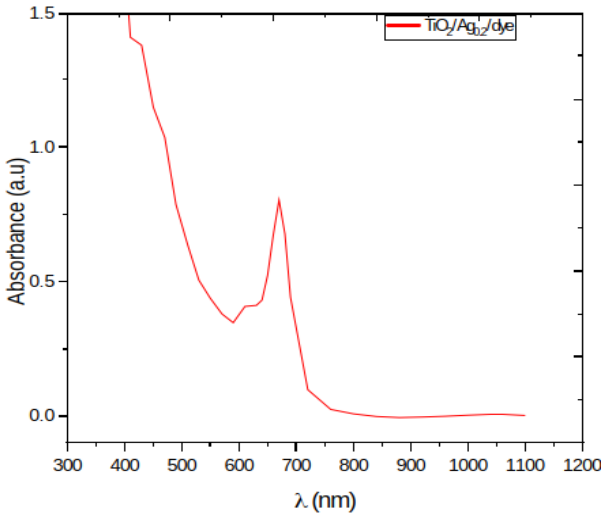

Figure 2: Absorbance spectra of dyes extracted from *Celosia argentea.*

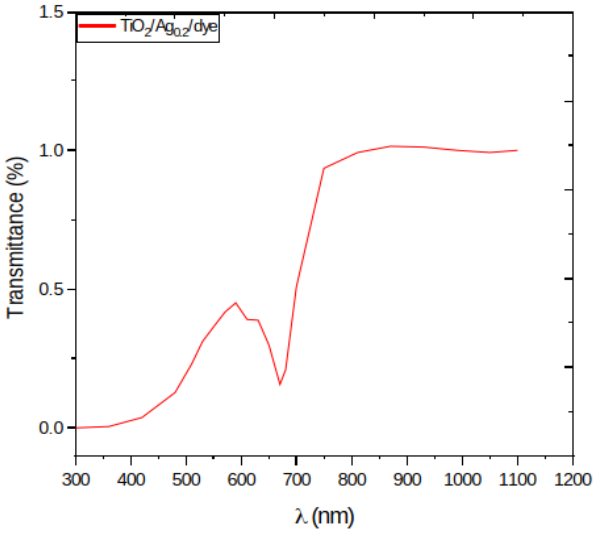

Figure 3: Transmittance spectra of dyes extracted from *Celosia argentea.*

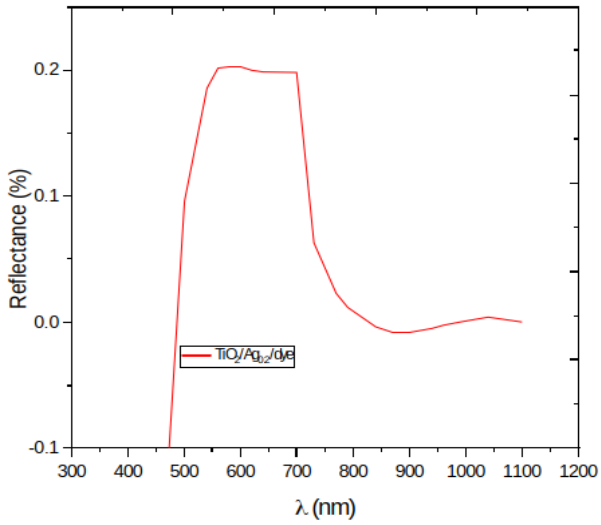

Figure 4: Reflectance spectra of dyes extracted from *Celosia argentea.*

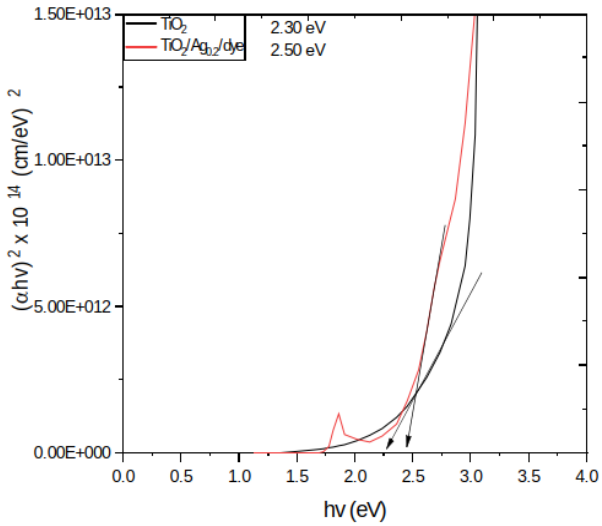

Figure 5: Energy band gap diagram of dyes extracted from *Celosia argentea.*

The reflectance spectra of TiO_2 and TiO_2/$Ag_{0.2}$/dyes are shown in Figure 4. The reflectance increases in the visible light region, then decreases in the NIR region, with a peak at about 752 nm. Maximum reflectance occurs at about 480-590 nm because the physical colour of the dye pigment is green, so it reflects green light. In summary, reflectance is low across the UV and NIR region of the electromagnetic spectrum.

Figure 5 shows the estimation of the band gap energy of dye-sensitized material and silver-doped TiO_2 by extending the linear part of the Tauc plots. Since the absorption coefficient (α) can be stated, this can be accomplished as: $\alpha hv=(hv-E_g)^2$. The optical energy band gap can be accurately estimated from the

intercept on the horizontal axis, where Eg, hv, α, and A represent the energy band gap, photon energy, absorption coefficient, and constant, respectively. The results showed that the optical band gap was 2.30 eV for TiO_2 and 2.50 eV for the Celosia argentea dye. The energy band gap is often determined by carrier concentration and the quantum-size effect [40].

4.2. Surface morphologyorphology

The synthesized TiO_2 and $TiO_2/Ag_{0.2}$/dye, as shown in Figure 6, reveal that the TiO_2 surface shows nano-scale growth of a few clouded nanoparticles. TiO_2 is well deposited on the surface of the FTO substrate. The deposition of silver (Ag) and dye onto TiO_2 resulted in a complete alteration of its surface energy. The surface of the synthesized material shifted from clouded nanoparticles to cluster nanoparticles, as observed in the micrograph of celosia leaf dye in the film. TiO_2, silver, and a dye enhance the surface energy of the synthesized material for solar and photovoltaic applications. The thickness of the TiO_2 on the FTO glass was measured to be approximately 102 nm, and the $TiO_2/Ag_{0.2}$/dyes film was approximately 106.25 nm.

The EDX spectra of the synthesized TiO_2 and $TiO_2/Ag_{0.2}$/dye are shown in Figure 7. EDX spectra were performed to determine the elements present in the materials. The synthesized FTO showed distinct peaks for titanium, oxygen, silicon, and calcium in the bare TiO_2 and $TiO_2/Ag_{0.2}$/dye mesoporous films.

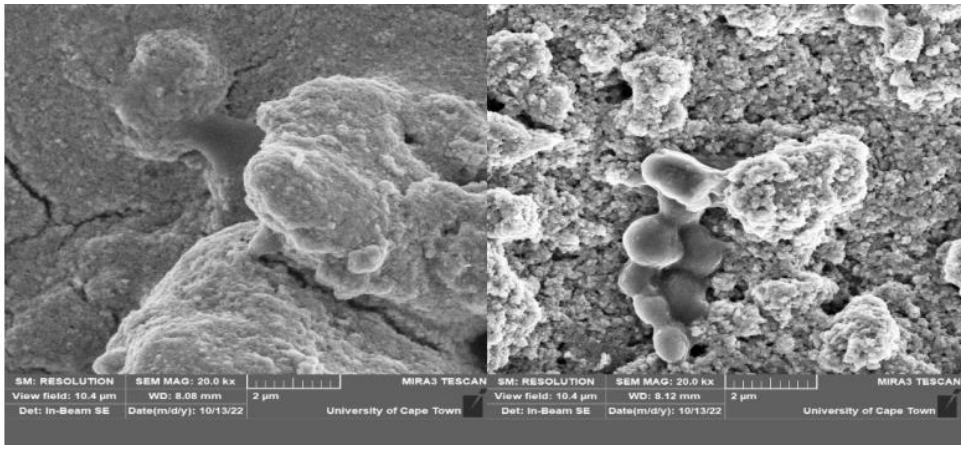

Figure 6: SEM micrograph of TiO_2 and $TiO_2/Ag_{0.2}$/dyes.

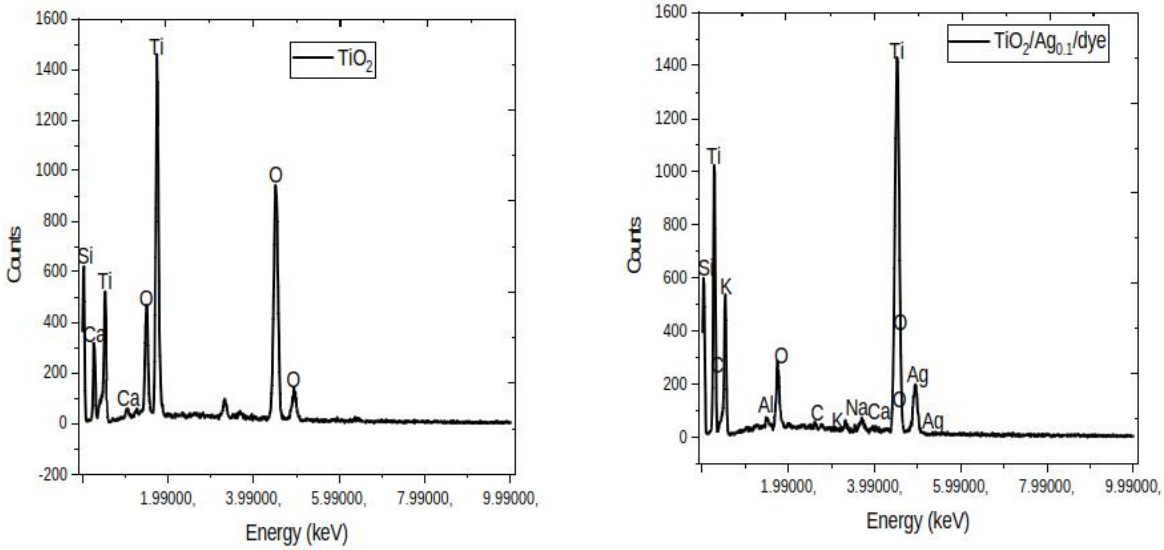

Figure 7: EDX spectrum of TiO_2 and $TiO_2/Ag_{0.2}$/dyes.

Titanium (Ti) has the greatest peak, followed by oxygen (O), with respect to all other elements present in the bare TiO_2. The peaks shown in the figure represent the concentrations of the various elements present due to the dye pigments and dopants' thorough absorption. The presence of potassium, calcium, carbon, Aluminum, sodium, and silver at lower concentrations in the TiO_2/$Ag_{0.2}$/dyes indicates the presence of a dopant and, likely, impurities. The spectrum shows that all the elements composing the TiO_2 mesoporous film are present.

4.3. Structural characterization

The Structural variables of TiO_2 and $TiO_2/Ag_{0.2}$/dye are shown in Table 1, while XRD analysis of the synthesized TiO_2 and $TiO_2/Ag_{0.2}$/dye is shown in Figure 8. The cells' structure is polycrystalline and shows prominent peaks at 2θ values of 30.375 and 29.397, corresponding to the (200) planes of the synthesized TiO_2 and the $TiO_2/Ag_{0.2}$/Celosia leaf dye. Other peaks were noticed at 2θ angles of 24.891°, 27.509°, 32.915°, 27.509°, 35.296°, 38.814°, 43.152°, 47.579°, 53.231° and 59.130° for TiO_2 and 24.229°, 26.768°, 29.397°, 34.229°, 36.195°, 42.094°, 45.454°, 50.197° and 61.343° for $TiO_2/Ag_{0.2}$/celosia leaf which corresponds to plane (101), (004), (105), (211), (116), (220), (215) and (303) respectively. The peak intensity is higher due to the enhanced crystal structure and energy absorption on TiO_2's lattice parameters. The peak locations remained unchanged even with the crystals' energy absorption. The dye distorts the lattice and individual cells, leading to shifts in crystal orientation. Equation 10 was used to compute the crystallite (grain) size. The films' crystallinity is enhanced by larger grains, as shown in Table 1 for TiO_2 and $TiO_2/Ag_{0.2}$/celosia leaf.

Table 1: Structural variables of TiO_2 and $TiO_2/Ag_{0.2}$/dye.

Films	2θ (°)	d-spacing (Å)	FWHM	(hkl)	Lattice constant a (A)	Dislocation density (δ)	Grain Size (D) nm
TiO_2	24.891	3.573	0.109	101	6.190	1.795	1.302
	27.509	3.239	0.112	004	6.478	1.875	1.274
	30.375	2.939	0.113	200	5.879	1.884	1.271
	32.915	2.718	0.114	105	6.079	1.893	1.268
	35.296	2.540	0.117	211	6.222	1.969	1.243
	38.814	2.317	0.119	204	6.556	1.996	1.235
	43.152	2.094	0.120	116	5.924	1.973	1.242
	47.579	1.909	0.123	220	6.332	2.007	1.231
	53.231	1.719	0.127	215	5.955	2.042	1.221
	59.130	1.560	0.129	303	5.840	1.994	1.235
$TiO_2/Ag_{0.2}$/celosia leaf	24.229	3.669	0.110	101	6.356	1.832	1.289
	26.768	3.327	0.111	004	6.654	1.847	1.284
	29.397	3.035	0.112	200	6.070	1.859	1.279
	34.229	2.617	0.113	105	5.852	1.848	1.283
	36.195	2.479	0.114	211	6.073	1.860	1.279
	39.634	2.271	0.116	204	6.425	1.887	1.270
	42.094	2.144	0.121	116	6.065	2.020	1.227
	45.454	1.993	0.122	220	6.611	2.006	1.232
	50.197	1.815	0.123	215	6.290	1.965	1.244
	61.343	1.509	0.123	303	5.649	1.773	1.310

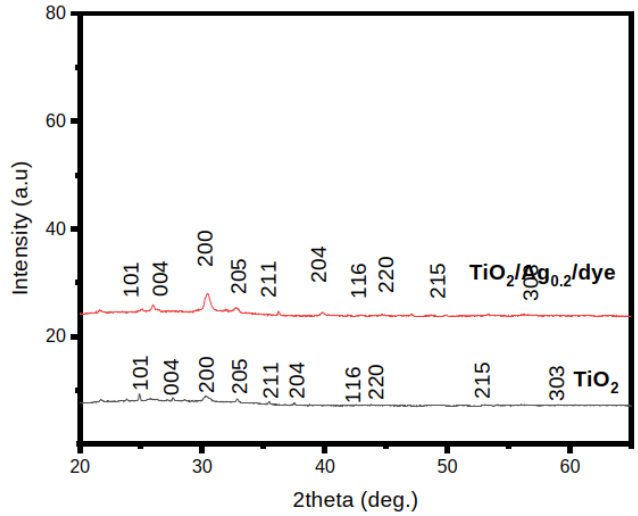

Figure 8: XRD pattern of TiO_2 and$TiO_2/Ag_{0.2}$/dye.

Table 2: Photochemical parameters of the fabricated DSSC.

Sensitized film	V_{oc} (V)	I_{sc} (mA/cm^2)	V_{max} (V)	I_{max} (mA/cm^2)	P_{max} (mW/cm^2)	FF	η (%)
$TiO_2/Ag_{0.2}$/Celosia dye	0.452	0.692	0.324	0.501	0.162	0.52	0.16

4.4. Photovoltaic/photoelectrochemical characterization

I-V curve of solar cell sensitized with the dye extract from *Celosia argentea* (Shoko leaf) Using the I-V characteristic curve of Figure 9, we were able to extract and summarize the photoelectrochemical parameters of the cell, as shown in Table 2.

The photovoltaic performance of DSSCs fabricated using *Celosia argentea* as a good sensitizer for TiO_2/ $Ag_{0.2}$ was assessed. The result revealed a PCE (η) of 0.16%; V_{oc} of 0.452 V, I_{sc} of 0.692mA/cm^2, V_{max} of 0.324 V, I_{max} of 0.501 mA/cm^2, P_{max} of 0.162 mW/cm^{2,} and FF of 0.52 were obtained. The coated FTO glass with a TiO_2 metal oxide surface, doped with silver at 0.2 molar concentration, has been shown to provide more surface area for dye adsorption, as evidenced by the peak observed in the absorbance spectra in Figure 2. This leads to higher dye concentration and photo-conversion efficiency (PCE) than reported for some undoped natural dye pigments [43-45].

5. Conclusion

A dye-sensitized solar cell was fabricated using a natural chlorophyll pigment extract from dried Celosia argentea, a commonly grown leaf in the Western part of Nigeria. The extracted dye was characterized optically using a UV-Vis Spectrometer. The surface morphology and structural properties of the sensitized film were studied using a Scanning Electron Microscope (SEM) and an X-ray diffractometer (XRD), respectively. The J-V characteristics were measured, and the photovoltaic properties were investigated. The PCE reached 0.16 % Voc of 0.452 V, Isc of 0.692 mA/cm^2, Vmax of 0.324 V, Imax of 0.501 mA/cm^2, Pmax of 0.162 mW/cm^2, and FF of 0.52. As revealed in these results, it is evident that the dye extract of *Celosia argentea* serves as a potent sensitizer for DSSC application.

6. References

1. Ezeh IM, Enaroseha OOE, Agbajor GK, Achuba FI. Effect of titanium oxide (TiO_2) on ntural dyes for the fabrication of dye-sensitized solar cells. Eng Proc. 2024;63:25.https://doi.org/10.3390/engproc2024063025.
2. Odia OB, Enaroseha OO, Robert OO, Ojegu EO, Ikhioya IM, Ekpekpo A, Osiele OM. Fabrication of dye-sensitized solar cells using nitrogen doped carbon quantum dots and organic dye extracted from purple

cabbage. Int J Adv Sci Technol. 2024;9(2):16-27.https://bwjournal.org/index.php/bsjournal/article/view/1747.
3. Osolobri BU, Enaroseha OOE, Omoyibo SE. Performance evaluation of dye-sensitized solar cell using bougainvillea flower extract. Int J Appl Phys Sci 2023; 9:42-47. https://dx.doi.org/10.20469/ijaps.9.500 05.
4. Hosseinnezhad M, Moradian S, Gharanjig K. Synthensis and application of two organic dyes for dye sensitized solar cells. Prog Color Colorant Coat. 2013;6(2):109-117. https://doi.org/10.30509/PCCC. 2013.75808
5. Etula J. Comparison of three Finnish berries as sensitizers in a dye sensitized solar cell. Eur J Young Sci Eng. 2012;1: 77-84 .
6. O'Regan B, Gratzel M. A low cost, high efficiency solar cell based on dye sensitized colloidal TiO_2 films. Nature. 1991;353:737-740. https://doi.org/10.1038/35 3737a0.
7. Mahmood A, Hussain Tahir M, Irfan V, Al-Sehemi V, Al-Assiri V. Heterocyclic azo dyes for dye sensitized solar cells: A quantum chemical study. Comput Theor Chem. 2015;1066:94-99. https://doi. org/10.1016/j. comptc.2015.05.020.
8. Kumara NTRN, Ekanayake P, Lim A, Liew LYC, Iskandar M, Ming LC, Senadeera GKR. Layered co-sensitization for enhancement of conversion efficiency of natural dye sensitized solar cells. J Alloys Compd. 2013; 581:186-191. https://doi.org/10.1016/j.jallcom.2013.07. 039.
9. Osolobri BU, Enaroseha OOE, Anho LO. Fabrication of dye-sensitised solar cell using dry Ixora extract as sensitizer. Mater Res Innov. 2025;29(3):135-142. https://doi.org/10.1080/14328917.2024.2389355.
10. Amaghionyeodiwe CA, Obi AI, Nwankwojike BN, Alu NO, Odili EP. Optical characteristics and bandgap analysis of Canarium Schweinfurthii, Telfaira Occidentalis and Curcuma Longa extract as natural sensitizers for the production of dye-sensitized solar cells. Niger Agric J. 2019;50(2):205-212. https://www.ajol.info/index.php/naj/article/view/196137/185156.
11. Okunzuwa GI, Enaroseha OOE, Okunzuwa SO. Synthesis and characterization of Fe(III) chitosan nanoparticles n-benzaldehyde Schiff base for biomedical application. Chem Pap. 2024;78(5):3253-3260. https://doi.org/10.1007/s11696-024-03309-5.
12. Aigbe UO, Onyancha RB, Ukhurebor KE, Okundaye B, Aigbe E, Enaroseha OOE, Obodo K, Osibote OA, El Nemr A, Noto LL, Atagana HI. Utility of magnetic nanomaterials for theranostic nanomedicine. In: Magnetic nanomaterials: synthesis, characterization and applications. Aigbe U.O., Onyancha R.B., Ukhurebor KE, (eds.), Magnetic Nanomaterials. Engr Mater. 2023; Chapter 3:47-86. https://doi.org/10.1007/978-3-031-36088-6_3.
13. Hoerner LJ. Photosynthetic solar cells using chlorophyll and the applications towards energy sustainability. USFSP Honors Program Theses (Under-graduate). 2013;136. http://digital.usfsp.edu/honorstheses/136.
14. Supriyanto E, Kartikasari HA, Alviati N, Wiranto G. Simulation of dye -sensitized solar cells performance for various local natural dye photosensitizers. IOP Conf Ser Mater Sci Eng. 2019; 515 (201):012048. https://doi.org/10.1088/1757-899X/515/1/012048.
15. Sharma K, Sharma V, Sharma SS. Dye-sensitized solar cells: Fundamentals and current status. Nanoscale Res Lett. 2018;13:381. https://doi.org/ 10.1186/s11671-018-2760-6.
16. Ojegu E, Enaroseha OOE. Optical properties of the anatase phase of titanium dioxide thin films prepared by electrostatic spray deposition. Nig J Sci Environ. 2020;18:120-124.
17. Wante HP, Yap SL, Aidan J, Alkasim A. Fabrication of dye-sensitized solar cell using flexible non- conductive polyetherimide (PEI) polymer substrate. J Mater Environ Sci. 2020; 11(10):1744-1753.
18. Enaroseha OOE, Ifayefunmi OS, Oyebola OO. Rate equation analysis of the 2.9 μm Holmium-Doped Potassium Lead Bromide (Ho:KPb2Br5) transition for diode laser application. J. Nig. Ass. Math. Phys. 2016; 37: 301-306. https://doi.org/10.31219/osf.io/6pyur.
19. Akila Y, Muthukumarasamy N, Velauthapillai D. Chapter 5-TiO_2-based dye-sensitized solar cells. In: Thomas S, Sakho EHM, Kalarikkal N, Oluwafemi SO, Wu J. (eds.) Nanomaterials for Solar Cell Applications: Elsevier; 2019;127-144. https://doi. org/10.1016/B978-0-12-813337-8.00005-9.
20. Ramanathan R, Zinigrad M, Kasinathan D, Poobalan RK. Zinc Stannate (Zn_2SnO_4)-based hybrid composite photoanode for dye-sensitized solar cell application. ACS Appl Energy Mater. 2022; 5(9):11506-11516. https://doi.org/10.1021/acsaem.2c01981.
21. Kumar Y, Chhalodia T, Bedi PKG, Meena PL. Photoanode modified with nanostructures for efficiency enhancement in DSSC: a review. Carbon Lett. 2023;33 (1):35-58. https://doi.org/10.1007/s42823-022-00422-x
22. Malumi SO, Malumi T, Osiele MO, Ekpekpo A, Ikhioya IL. Enhance and performance evolution of silver-doped titanium dioxide dye-sensitized solar cells using different dyes. J Eng Ind Res. 2023;4(4): 189-200.https://doi.org/10.48309/jeires.2023.4.1.
23. Malumi SO, Osiele MO, Enaroseha OOE, Daniel-Umeri R, Chukwu JO. Performance evaluation and characterization of fabricated silver nitrate doped DSSC sensitized with dye extracted from Corchorus olitorius L. Nig J Sci Environ. 2024;22(3):59-73. https://doi.org/10.61448/njse223245.
24. Aigbe UO, Ukhurebor KE, Onyancha RB, Okundaye B, Aigbe E, Obodo K, Enaroseha OOE, Noto LL, Osibote AO, Atagana HI. Activated biosorbents for the removal of metals from aqueous solutions., Ukhurebor KE, Aigbe, UO., Onyancha R.B (eds.), Adsorption applications for environmental sus-tainability, 2023; Chapter 3:3.1-3.27. https://doi.org/ 10.1088/978-0-7503-5598-8ch3
25. Okunzuwa IG, Enaroseha OOE, Okunzuwa SI, Omajale SO, Oyibo O. Preparation and charac-terization of chitosan furfural schiff base in the removal of Aqueous 2,4-Dinitrophenol. Int J Appl Phys Sci. 2024; 10:15-21. https://dx.doi.org/10.20469/ ijaps.10.50002.
26. Mahalingam S, Abdullah H. Electron transport study of

indium oxide as photoanode in DSSCs: A review. Renew. Sustain. Energy Rev. 2016;63:245-55. https://doi.org/10.1016/j.rser.2016.05.067.
27. Shakeel AM, Pandey AK, Abd RN. Advancements in the development of TiO_2 photoanodes and its fabrication methods for dye sensitized solar cell (DSSC) applications A review. Renew. Sustain. Energy Rev. 2017; 77:89-108. https://doi.org/10.1016/ j.rser.2017.03.129.
28. Amarsingh BK, Kalpana DA, Theerthagiri J, Madhavan J, Balu T, Rajasekaran TR. Tungsten doped titanium dioxide as a photoanode for dye sensitized solar cells**.** J Mater Sci Mater Electron. 2017; 28(4):3428-39. https://doi.org/10.1007/s10854-016-5940-0
29. Ahamed S, Shekshavali T, Syed SR. Celosia argentea: A Review. Res J Pharmacol Pharmacodyn. 2018; 10(2): 83-86. https://doi.org/10.5958/2321-5836.2018.00015.0.
30. Filip MS, Macocian EV, Toderaş AM, Cărăban A. Spectrophotometric measurements techniques forfermentation process (part one) base theory for UV-Vis spectrophotometric measurements. Internal Report. 2012;78:34.
31. Enaroseha OOE, Apanapudor JS, Oyibo O, Oho MO. Understanding the theoretic study of alkali metal (Sodium, Na) properties from ab initio calculations. J. Phys. Conf. Ser. 2024; 2780:012030. https://doi.org/10.1088/1742-6596/2780/1/012030.
32. Yousaf SA, Abass JM. Structural, morphological, and optical characterization of SnO_2: F thin films prepared by chemical spray pyrolysis. Int Lett Chem Phys Astron. 2013;13(2):90-102. https://doi.org/10.18052/WWW.SCIPRESS.COM/ILCPA.18.90.
33. Maurya IC, Gupta AK, Srivastava P, Bahadur L. Natural dye extracted from Saraca asoca flowers as sensitizer for TiO_2 -based dye-sensitized solar cell**.** J. Sol. Energy Eng.2016;138(5):051006. https://doi.org/10.1115/1.4034028
34. Hossein BM. Performance of nano structured dye-sensitized solar cell-utilizing natural sensitizer operated with platinum and carbon coated counter electrode. Dig J Nanomater Biostruct. 2009;4(4):723-727 https://www.chalcogen.ro/723_Hossein.pdf.
35. Kim JJ, Kang M, Kwak OK, Yoon Y, Min KS, Moo-Jung C. Fabrication and characterization of dye-sensitized solar cell for greenhouse application. Int J Photoenergy. 2014;1-7. https://dx.doi.org/10.1155/ 2014/ 376315.
36. Bera S, Sengupta D, Roy S, Mukherjee k. Research into dye sensitized solar cells: a review highlighting progress in India. J Phys Energy. 2021;3(3):032013. https://doi.org/10.1088/2515-7655/abff6c.
37. Senthil T, Muthukumarasamy N, Kang M. ZnO nanorods based dye sensitized solar cells sensitized using natural dyes extracted from Beetroot, Rose and Strawberry**.** Bull Korean Chem Soc. 2014;35(4): 1050-1056. http://dx.doi.org/10.5012/bkcs.2014.35.4. 1050.
38. Kabir F, Bhuiyan MMH, Manir MS, Rahaman MS, Khan MA, Ikegami T. Development of dye sensitized solar cell based on combination of natural dyes extracted from Mabalar spinach and red spinach. Result Phys. 2019;19:102474 https://doi.org/10.1016/j.rinp.2019.102474.
39. Kakiage K, Aoyama Y, Yano T, Oya K, Fujisawa J, Hanaya M. High efficient dye sensitized solar cells with collaborative sensitization by silyl-anchor and carboxy-anchor dyes. Chem. Commun. 2015; 88(1): 420-435. https://doi.org/ 10.1039/c5cc06759f.
40. Sanusi A, Moreh AU, Hamza B, Sadiya U, Abdullahi Z, Wara MA, Kamaluddeen H, Kebbe MA, Monsurat UF. Optical characterization of Fluorine doped Tin Oxide (FTO) thin films deposited by spray pyrolysis technique and annealed under Nitrogen atmosphere. Int J Innov Appl Stud. 2014;9(2):947-955. https:// ijias.issr-journals.org/abstract.php?article=IJIAS-14-240-02.
41. Jihuai W, Lan Z, Lin J, Huang M, Fan L, Luo G, Lin Y, Xie Y, Wei Y. Counter electrode in dye sensitized solar cells. Chem Soc Rev. 2017; 46(19): 5975-6023. https://doi.org/10.1039/C6CS00752J.
42. Masud H, Kim K, Redox shuttle-based electrolytes for dye-sensitized solar cells: comprehensive guidance recent progress and future perspective. ACS Omega. 2023;8(7):6139-6163. https://doi.org/10.1021/acsome ga. 2c06843.
43. Ammar AM, Abdel-Hafez GM, Mohamed HSH, Hassanien AS, Yousef MMK, Khalil ASG. Dye-sensitized solar cells (DSSCs) based on extracted natural dyes. J Nanomater. 2019;10(1):69-77. https://doi.org/10.1155/2019/1867271.
44. El-Ghamri HS, El-Agez TM, Taya SA, Abdel-Latif MS, Batniji AY. Dye-sensitized solar cells with natural dyes extracted from plant seeds. Mater Sci Pol. 2014; 32(4):547-554. https://doi.org/10.2478/s13536-014-0231-z.
45. Chang H, Wu HM, Chen TL, Huang KD, Jwo CS, Lo V. Dye sensitized solar cell using natural dyes extracted from spinach and ipomoea. J Alloys Compd. 2010;495 (2):606-610.https://doi.org/10.1016/j.jallcom.2009.10.057.

How to cite this article:
Onyeka Malumi S, Enaroseha OOE, Cynthia Nnanna A, Oyibo O, Blessing Umukoro A, Daniel-Umeri R. Photovoltaic Performance of Photoelectric Dye Sensitized Solar Cell Using Silver Nitrate Doped Titanium Oxide ($AgNO_3$-TiO_2) Nanoparticles as Photoanode Electrode. Prog Color Colorants Coat. 2026;19(3):351-361. https://doi.org/10.30509/pccc.2025.167687.1457.